Available online at www.sciencedirect.com
SCIENCE DIRECT®
ELSEVIER
Nuclear Instruments and Methods in Physics Research A 538 (2005) 206–217
NUCLEAR INSTRUMENTS & METHODS IN PHYSICS RESEARCH Section A
www.elsevier.com/locate/nima

R&D of copper beam duct with antechamber scheme for high-current accelerators

Y. Suetsugu[a,*], K. Kanazawa[a], K. Shibata[a], H. Hisamatsu[a], K. Oide[a], F. Takasaki[a], A.E. Bondar[b], V. Kuzminykh[b], A. Gorbovsky[b], R. Dostovalov[b], K. Sennyu[c], H. Hara[c]

[a]*High Energy Accelerator Research Organization (KEK), 1-1 Oho, Tsukuba, Ibaraki 305-0801, Japan*
[b]*Budker Institute of Nuclear Physics (BINP), Novosibirsk 630090, Russia*
[c]*Mitsubishi Heavy Industries Co. Ltd., Kobe 652-8585, Japan*

Received 20 May 2004; received in revised form 14 September 2004; accepted 17 September 2004
Available online 19 October 2004

Abstract

A beam duct with an antechamber scheme for high-current accelerators was designed and the test chambers were studied experimentally. The duct consists of two channels, i.e., a beam channel where a beam circulates and a Synchrotron Radiation (SR) channel (antechamber) aside where the SR passes through. By using the antechamber scheme, the maximum power density of SR can be diluted at the side wall. The impedance is small owing to the pumping ports not being at the beam channel, but at the SR channel. Photoelectrons inside the beam channel are also expected to be reduced, which would be a big merit for a positron ring to suppress the electron cloud effect since the photoelectron is a major source of electrons composing the cloud. Two copper test chambers were manufactured with different methods, by pressing and by drawing. These chambers showed a good static vacuum property, i.e., gas desorption rates with less than 3.5×10^{-9} Pa m^3 s^{-1} m^{-2} after baking. After the installation to the positron ring of the KEK B-factory (KEKB), electron numbers in the beam channel, temperatures and pressures were measured during beam operation. The electrons in the beam channel were found to be reduced by a factor of 4 at 1.5 A compared to the case of the usual circular chamber. The reduction, however, was much larger, about 1/300, at a beam current of about 20 mA where the photoelectrons were dominant and the multiplication of electrons by the multipactoring was small. The temperatures were almost in agreement with the expectation. Vacuum scrubbing by photons proceeded almost smoothly, although pressure bursts were sometimes observed, especially for one test chamber, which was possibly due to discharges at the transverse joints in the beam chamber. Various instructive information had been obtained for future practical beam ducts for high-intensity accelerators.

PACS: 29.; 29.20.−c

Keywords: Accelerator; Vacuum; Beam duct; High current; Photoelectrons

*Corresponding author. Tel.: +81 298645227; fax: +81 298643182.
E-mail address: yusuke.suetsugu@kek.jp (Y. Suetsugu).

0168-9002/$ - see front matter © 2004 Elsevier B.V. All rights reserved.
doi:10.1016/j.nima.2004.09.015

1. Introduction

For high-intensity electron/positron colliders aiming for a luminosity of above $1 \times 10^{35}\,cm^{-2}\,s^{-1}$, the stored beam current goes up to about 10 A [1,2], which is larger by a factor 5 than that of the factory machines operating at present, such as KEK-B factory (KEKB) [3,4] or PEP II [5]. The resultant power of synchrotron radiation (SR) is much higher than that experienced so far. For the vacuum system of such a high-intensity machine therefore, the temperature and the thermal stress of the beam duct due to the high SR power density becomes a major problem. The large gas load due to the photon numbers should also be considered. The impedance of the beam duct is another important concern, since it leads to an intense excitation of higher-order modes (HOM) and strong beam instabilities under high-current operation.

Proposed here is a beam duct adopting an antechamber scheme for high-intensity accelerators [6,7]. The duct consists of two channels: one is the beam channel for a circulating beam, and the other is an SR channel (antechamber) for the SR. The schematic structure of the beam duct is shown in Fig. 1. The first advantage of the beam duct with the antechamber scheme is that it can reduce the maximum power density of SR on the side wall. The chamber has a wide outer half-aperture and the maximum power density of the SR is diluted due to its vertical spread at least. If the first SR from a bending magnet hit the outside of the magnet, the horizontal spread can also contribute to reduce the maximum power density. The maximum SR power density is an important parameter in considering the mechanical property of a beam duct. Typical operating parameters of the KEKB positron ring during our experiment and the values relevant to SR are listed in Table 1. The second merit is the small beam impedance. Since the pumping channels are at the SR channel, the effect of pumping slots (holes) on the beam becomes small. Furthermore, the antechamber can also reduce the photoelectrons density in the beam channel because the antechamber confines them. This would mitigate the electron cloud effect on the positron beam since the photoelectron is a major source of electrons composing the cloud. Even if the electrons multiplied by the multipactoring should be dominant, the photoelectrons can be the origin of those. The structure of the beam duct, however, becomes rather complicated compared to the usual circular or semi-circular ones.

In anticipation of future practical applications, two copper test chambers with the antechamber scheme were manufactured with different methods. One is by pressing from copper plates, and another is by the drawing of a copper pipe. The ultimate pressure and the residual gas components of the test chambers were measured after baking.

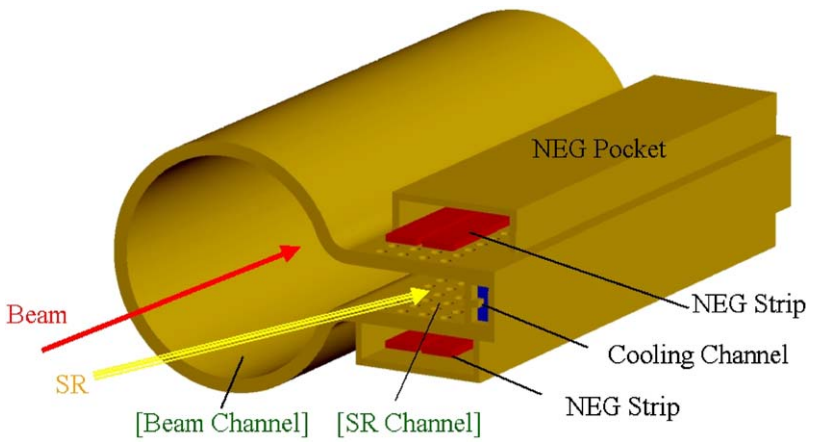

Fig. 1. Schematic drawing of a beam duct with an antechamber scheme.

Table 1
Main parameters of KEKB LER (positron ring) during our experiment and related SR values at a beam current of 1.5 A [8]

Beam energy	3.5	GeV
Max. beam current	1.5	A
Typical bunch number	1284	
Bunch length (σ)	6	mm
Bending radius	16.31	m
Length of bending magnet	910	mm
Critical energy of SR	5.8	keV
Max. SR line power density	8.5[a] (4.6[b])	$kW\,m^{-1}$
Max. SR power density	22.5[a] (6.4[b])	$W\,mm^{-2}$
[Vertical height ($=2/\gamma$)]	[0.38[a] (0.71[b])]	[mm]
Maximum photon line density	1.9×10^{19}[a] (1.0×10^{19}[b])	photons $m^{-1}\,s^{-1}$

[a]Case of a half-aperture of 47 mm.
[b]Case of a half-aperture of 112 mm.

Test chambers were then installed and tested with the beam in the KEKB positron ring (Low Energy Ring, LER). The electron numbers in the beam channel, the temperatures of the chamber body and the pressure rise due to SR (the photon stimulated gas desorption) were measured during regular beam operation. The obtained results are useful in considering the next practical beam duct for future high-current accelerators.

2. Manufacturing of test chambers

Two test chambers, Type-1 and Type-2, were manufactured for this study. Whole drawings of both types are presented in Fig. 2. Both chambers are made of oxygen-free copper. Copper is a suitable material for the beam duct of high-current accelerators, since it has a high thermal conductivity and a relatively high thermal strength [8]. The total length is 5.142 m. The beam channel is circular with a diameter of 94 mm, which is the same as the present beam chamber of LER [8,9]. The total height of the SR channel is 18 mm, and the half-outer aperture of the beam chamber is 112 mm (the total horizontal aperture is 159 mm). A cooling channel is at the side wall of the SR channel. NEG pockets are above and below the SR channel (only at the bottom for Type-2). NEG strips with a width of 30 mm (ST707) are installed in the NEG pockets. The far upstream side of the chamber is in a bending magnet and has a curvature of 16.31 m as a whole.

The test chamber Type-1 consists of four units of short chambers (1.2–1.5 m). One unit is an assembly of two pressed plates (6 mm thick) and a cooling channel. These are axially welded by an electron beam, as shown in Fig. 3. A saw-tooth structure is machined on the surface of the cooling channel to reduce the photoelectron yield and the reflection of SR [10,11]. The pitch and depth of the saw-tooth are 5 and 0.5 mm, respectively. Two adjacent units were connected by a TIG welding at the stainless-steel parts of the two bi-metal (stainless-steel and copper) pieces, of which each copper part had been welded by an electron beam to the edge of the unit (see the drawing in Fig. 14 later). A copper RF-bridge coated by gold was sandwiched by these pieces to make the inner surface smooth. Unit-1 is bent with a curvature of 16.31 m as a whole. The two middle units (Unit-2 and -3) have NEG pockets at both the upper and lower parts of the SR channel. The diameters of the pumping holes in Unit-2 and -3 are 4 and 6 mm, respectively. The most downstream unit (Unit-4) has a port for an ion pump at the bottom of the SR channel. Unit-1 and -4 have tapers at the ends to connect to the usual circular beam chamber. A whole view is presented in Fig. 4.

A major problem found during the production of Type-1 was the steps inside the three joints of the units. The cause was a mismatch between the

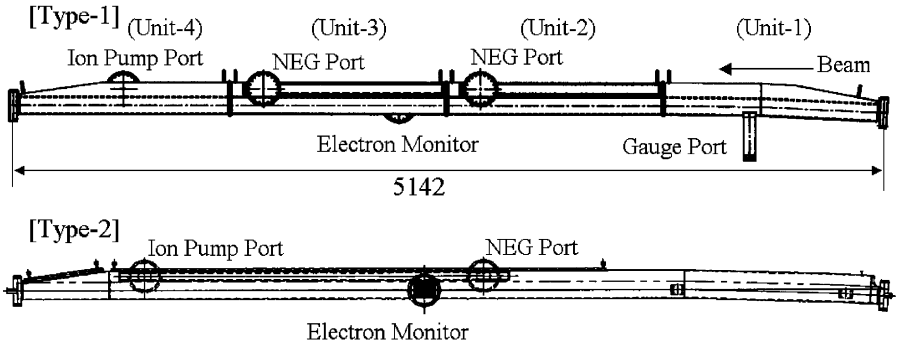

Fig. 2. Entire drawing of the two test chambers.

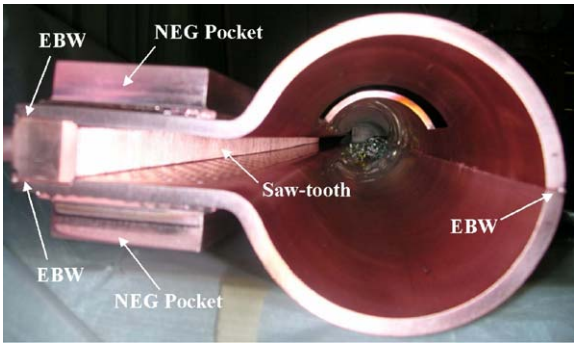

Fig. 3. Cross-section of the Type-1 test chamber.

Fig. 4. Entire view of the Type-1 test chamber.

machined RF-bridge and the actual cross-section of the chamber. The step at the beam channel is relatively small, since the control point of the alignment is at its side wall. The steps at the transition from the beam channel to the SR channel and in the SR channel are larger than that at the beam channel, and the height is 0.5–1.0 mm. No repair was made on the step this time.

Type-2 has almost the same cross-section and sizes as that of Type-1. The most different point of Type-2 from Type-1 is that the chamber is a drawn pipe with the final cross-section, except for the NEG pocket and the cooling channel. The cross-section of the drawn pipe of Type-2 is shown in Fig. 5. The thickness is uniform (6 mm). Holes for pumping were drilled from outside, and each has a diameter of 6 mm. The NEG pocket is at the bottom of SR channel only at the downstream side of the chamber. The ports for an ion pump and an electron monitor are also provided as in Type-1. Another feature of Type-2 is the copper-alloy (Cu–0.7%Cr–0.07%Zr) flange at the ends. The copper-alloy flange makes it possible to weld the flange to the beam chamber directly. A complete view of Type-2 is presented in Fig. 6.

The side wall of the SR channel has a rough surface with Ra $\approx$ 10 μm, which is formed by a glass beads blast (GBB) method. Since the beam chamber is a long drawing pipe, machining of saw-tooth structure, as in the case of Type-1, is impossible. The reduction of the photoelectron yield by the rough surface was checked in advance using a beam line at the Photon Factory of KEK [11]. The reduction was almost the same as that of a saw-tooth structure within a factor of 2.

Fig. 5. Cross-section of the Type-2 test chamber.

Fig. 6. Entire view of the Type-2 test chamber.

Note that both the saw-tooth in Type-1 and the rough surface in Type-2 increase the SR line power density, although they can reduce the photoelectron yield. Especially, the saw-tooth surface should increase the density by several factors. This is not a problem in the test using the present KEKB, but may be an issue in the future high-current machine. A more detailed thermal analysis and a careful design should be required in that case.

The two manufacturing methods have merits and demerits, respectively. A main future issue of the pressing method (Type-1) is to improve the accuracy of forming. The steps inside the joints of the units, or at the welding points of the flanges will be mitigated by increasing the accuracy. The reliability of a large number of vacuum-tight welding lines may be another concern, considering the necessary number of chambers, about 1000, for example. Lengthening a unit should be another issue in practical cases. Once an appropriate family of dies for pressing is prepared in mass production, the method may be rather easy. The drawing method (Type-2) has no critical problem, and seems to be suitable for manufacturing a relatively long chamber. Thanks to the drawing of a long pipe, there are fewer joints and no axial vacuum-tight welding line. The correction of bending and twisting after the drawing will be an issue for a long chamber.

3. Static vacuum properties

The static vacuum properties of the test chambers, Type-1 and Type-2, were examined. For Type-1, four NEG strips were installed from specified ports on the NEG pockets. After assembling and helium leak checking, the chamber was baked up to 150 °C for 24 h. The pumps included one turbo-molecular pump (TMP, STP-301, SEIKO SEIKI Co. Ltd., pumping speed $= 0.3\,m^3\,s^{-1}$) at one end, and four NEG strips (ST707, 1 m each) in the NEG pockets. The ultimate pressure was measured by an Extractor gauge (IONIVAC IM-520, Leybold Vakuum GmbH). The pressure, about 40 h after the baking, was about 2.1×10^{-8} Pa in N_2 equivalent. Assuming a total surface area of $3\,m^2$ (including four NEG pockets and seven ports) and a total pumping speed of $0.5\,m^3\,s^{-1}$, taking into account the conductance (TMP $= 0.1\,m^3\,s^{-1}$, NEG strips $= 0.4\,m^3\,s^{-1}$), the gas-desorption rate is about $3.5 \times 10^{-9}\,Pa\,m^3\,s^{-1}\,m^{-2}$. The gas desorption rate is sufficiently small. The main residual gases are H_2, followed by H_2O, CO and CO_2. The composition is a typical one for a baked copper chamber [12].

On the other hand, Type-2 has a NEG pocket, where a NEG strip with a length of about 1.5 m was installed. One lumped NEG pump was temporally added at the port for an electron monitor. The chamber was also baked at 150 °C

for 24 h. The rough pumping system and the vacuum gauges were the same as in the case of Type-1. The pressure 48 h after baking was 1.2×10^{-8} Pa. Assuming that the total surface area is about 2 m^2 (including one NEG pocket and three ports) and the total pumping speed is about 0.35 $m^3 s^{-1}$ (TMP $= 0.1\,m^3 s^{-1}$, lumped NEG $= 0.1\,m^3 s^{-1}$, NEG strip $= 0.15\,m^3 s^{-1}$), the gas-desorption rate is about 2.1×10^{-9} Pa $m^3 s^{-1} m^{-2}$ in N_2 equivalent. The residual gas components are almost the same as that of Type-1. The gas-desorption rate is about half that of the case of Type-1. This may come from the fact that Type-2 has fewer welding points compared to the case of Type-1 (NEG pockets, cooling channel, transverse and axial joints), or a difference in the surface treatment.

For both cases, the chamber showed a good static vacuum property, which was almost the same as that of the usual circular beam chambers produced for the KEKB so far [12].

4. Experiments in the LER

4.1. Installation and setup

The Type-1 was installed in LER in December 2003. The layout in the tunnel and the positions of various monitors are shown in Fig. 7. A bending magnet is at the upstream end of the chamber. The bending radius is 16.31 m and the beam energy is 3.5 GeV. The critical energy of photons is 5.84 keV. An electron monitor is attached on a port at the beam channel of Unit-3 [10]. The bias voltages at a repeller and a corrector of the monitor are -30 and $+100$ V, respectively. The effective aperture of the collector is about 250 mm^2. The electron monitor, therefore, can measure photoelectrons or secondary electrons in the beam channel with energies larger than 30 eV. Photoelectrons generated in the monitor port will be repelled, since their energy is almost less than 10 eV, unless any acceleration by beam occurs. The temperatures of three points on the chamber were measured. The temperatures of NEG strips at Unit-2 and -3 can also be measured directly during operation. Two vacuum gauges (cold cathode gauges) were set at just above the ion pump (Unit-4) and at the gauge port (Unit-1, inside of bending magnet). The chamber was not baked in the tunnel, but NEG strips were activated before starting beam operation. The solenoids were wound around the chamber after installation. The typical field strength is about 0.004 T in the axial direction.

The Type-2 was installed in LER in March 2004, following about three months of experiments using Type-1. The pump, gauge and electron monitor were the same as those used in Type-1. The temperature of the NEG strips and the pressure inside the bending magnet were not measured in this case. The chamber was also not baked in the ring. There had been no solenoid around the chamber from the beginning. The test chamber Type-2 installed in LER is presented in Fig. 8.

4.2. Electrons in the beam channel

The electron current was measured during regular operation. The bunch number was 1284 and the bunch spacing was almost 8 ns. The positron beam was stored up to about 1.5 A. The

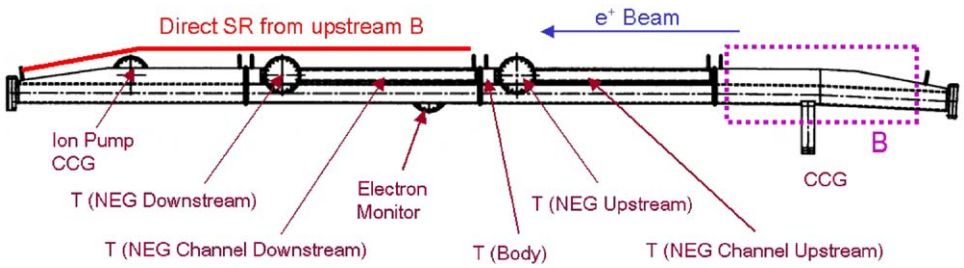

Fig. 7. Layout of the Type-1 test chamber in the tunnel and the setup of various monitors.

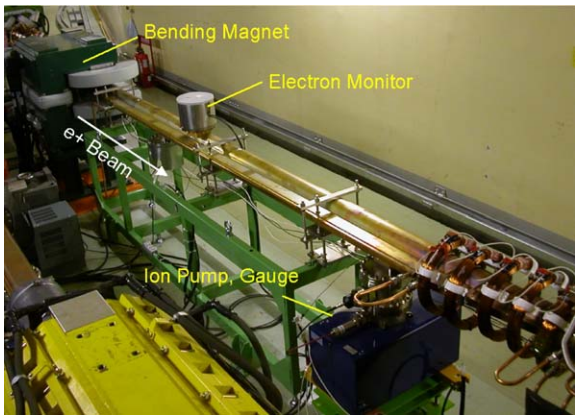

Fig. 8. Type-2 test chamber installed in LER.

photon flux near the monitor was 9.4×10^{18} photons s^{-1} m^{-1} at 1 A beam for the test chamber (half-aperture =112 mm), and almost the same as in the previous experiment using a normal circular chamber (half-aperture = 47 mm), 8.5×10^{18} photons s^{-1} m^{-1} at 1 A.

The measured electron current for Type-1 and Type-2 without a solenoid field are presented in Fig. 9(a) as a function of the beam current. The electron current measured with the usual circular chamber is also plotted in the same figure. Note that the lower limit of the measurement is 1×10^{-1} A. As can be seen in the figure, the electron current of the test chamber is less than that of the circular chamber as a whole, but the ratio changes greatly with the beam currents. The reduction rate is only about 1/4 at a beam current of 1.5 A, but is about 1/300 at around 20 mA. The electron current apparently shows a nonlinear behaviour against the beam current. If the electrons are only photoelectrons, the electron current should be in proportion to the beam current (the slope is 1 in logarithmic scale). The electrons of the usual circular chamber, therefore, are mainly photoelectrons. On the other hand, for the case of the test chamber, the slope of the curve is steeper than 1, and near 2 for a beam current higher than 100 mA. The steep slope means that a multiplication of electrons should occur at the high-current regime. In other words, the reduction rate is small at a high current, where the multiplication of electrons is

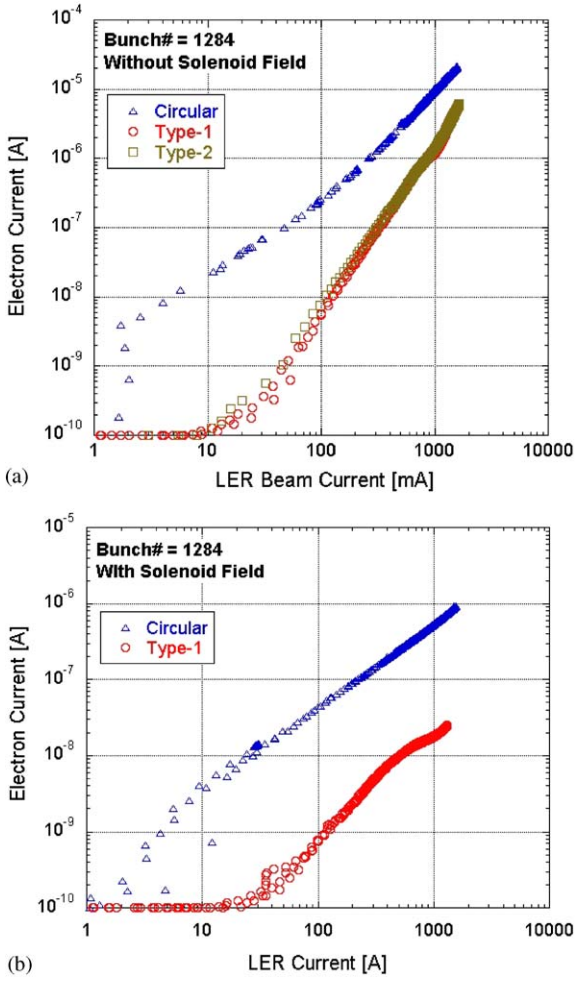

Fig. 9. Beam-current dependence of the electron current measured for test chambers Type-1 and Type-2, and the circular chamber (a) without and (b) with a solenoid field.

dominant, but is large at a low current where most electrons are photoelectrons.

The reduction rate of photoelectrons, about 1/300, is almost in agreement with our expectation. A simulation showed that the photoelectrons in the beam channel decreased by about 1/10 when using the antechamber scheme. Furthermore, a saw-tooth surface, or a rough surface on the cooling channel, reduces the photoelectrons by 1/20–1/10 [10,11]. Totally, the photoelectrons are expected to be reduced by about 1/100.

The reason why the multiplication of electrons is not as apparent for the circular chamber as for the test chamber may be explained as follows: the multipactoring is almost the same in both chambers but masked by the stronger photoelectron current without the solenoid field. This can be true if the condition of the multipactoring is not satisfied for most photoelectrons. Actually, there is some nonlinearity seen in the plot for the circular chamber at higher beam current, where the effect of multipactoring becomes much stronger. However, another possibility that cannot be completely eliminated is that some mechanism to suppress the multipactoring is working due to the dense photoelectrons in the circular beam duct. This depends on how much of photoelectrons can contribute to the multipactoring. Either way, a further experiment, a quantitative analysis of the data and also a detailed simulation are necessary in the future.

As a reference, the results with a solenoid field are presented in Fig. 9(b). One should be careful that the measured current does not directly reflect the electron number in the beam channel, since the orbit of electrons should be distorted by the solenoid field. The electrons entered in the collector are, therefore, those strongly accelerated by the beam, and those emitted inside of the monitor by scattered SR. However, it can be said, at least, that since the slope is almost one, the multiplication of electrons is almost suppressed by the solenoid field, and that the photoelectrons are dominant. Furthermore, the electron current for the test chamber is smaller by one order of magnitude than that of the usual circular chamber. This indicates the less-scattered SR in the beam channel, although an accurate, quantitative comparison is not very easy due to the different configuration of the solenoid field.

The reason for a bump near the beam current of 0.7 A, seen in both figures, has not yet been understood. However, it was found that the position of the bump changed with the bunch fill pattern of the stored beam. This means that the bump comes from a resonant phenomenon determined by the size of the beam chamber and the bunch spacing. Additional experimental and simulation studies are required.

It can be concluded that the beam duct with the antechamber scheme is very effective, but not perfect in reducing electrons in the beam channel at a high-current regime where the multiplication of electrons is likely to occur. The solenoid magnetic field or some coating on the inner surface to reduce the secondary electron yield should be indispensable for high-current operation to suppress the electron cloud effect completely [4].

4.3. Temperatures

The temperatures of the NEG pockets, the chamber body and the NEG strips were measured during beam operation. Fig. 10 shows typical behaviour of the temperatures during beam operation measured for Type-1. The temperature of the NEG pocket at the downstream side increased with the beam current up to about 40 °C, whereas that at the upstream side stayed at about 28 °C. Since the direct SR from the upstream bending magnet is irradiating only the downstream side (Unit-3 and -4), as indicated in Fig. 7, the larger temperature rise at the downstream side is reasonable.

The result of two-dimensional thermal analysis (static) is presented in Fig. 11 calculated by the ANSYS7.0 program. The input SR power density is 6.4 W mm^{-2}, the maximum power density at the beam current of 1.5 A (see Table 1). The temperature of the NEG pocket is about 33–35 °C. The measured temperature of 40 °C, therefore, is slightly higher than that of the simulation, taking into account only the power of SR. The temperature rise of the NEG pocket and the body at the upstream side and the body will be mainly due to the HOM excited due to the localized antechamber structure. Taking into account the effect of HOM (temperature rise of 3–5 °C), the temperature rise of the NEG pocket at the downstream side is almost in agreement with the simulation. For reference, the loss factor of two tapers at transitions from a circular pipe to an antechamber is about 5 V nC^{-1}, which causes a HOM power of about 200 W at 1.5 A. The temperatures of the Type-2 chamber were almost the same as the results measured above. An extra cooling channel at the opposite side of the SR channel, for

example, will be necessary for high-current operation.

The temperature of the NEG strip is almost the same as that of the NEG pocket even in the steady state. This means that the temperature rise of NEG is not due to the HOM inside of the NEG pockets, but due to heating of the chamber by SR. The material of NEG (Ti, Zr, V) has much lower electric conductivity compared to the NEG channel (Cu). If the HOM heating of the NEG strip is prominent, the temperature of the NEG should be higher than that of the NEG channel since the NEG strip is almost thermally insulated (supported by ceramics blocks). The temperature of NEG at the downstream side was higher than that at the upstream side, which was mainly due to the higher temperature of the NEG pockets, as described above. Actually, the diameter of the pumping holes at the downstream side (Unit-3) was larger than that of the upstream side (Unit-2) as described earlier. However, the effect of the difference of the hole diameter on the temperature rise is not clear at present.

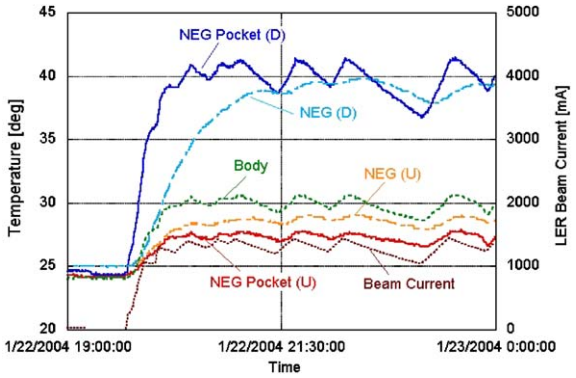

Fig. 10. Temperatures of the NEG pockets, the chamber body and the NEG strips during beam operation (Type-1).

4.4. Vacuum scrubbing

Fig. 12 shows the decreases of the pressure rises per unit of the beam current, $\Delta P/\Delta I$(Pa mA^{-1}), at the test chamber region for both types as a function of the integrated beam current, Beam Dose (mA h). The $\Delta P/\Delta I$ for a normal circular beam chamber in use for the KEKB is also plotted in the figure as a reference. The circular chamber had received the same baking procedure with the test chambers before installation. The $\Delta P/\Delta I$ of the test chambers decreased smoothly with the beam operation, and was almost the same as that of the circular chamber. At a beam dose of 2×10^5 mA h, the solenoid around the chamber was switched off in the case of Type-1. At that point, the pressure increased by one order of magnitude. This is because a multipactoring began by switching off the solenoid in the beam channel and the

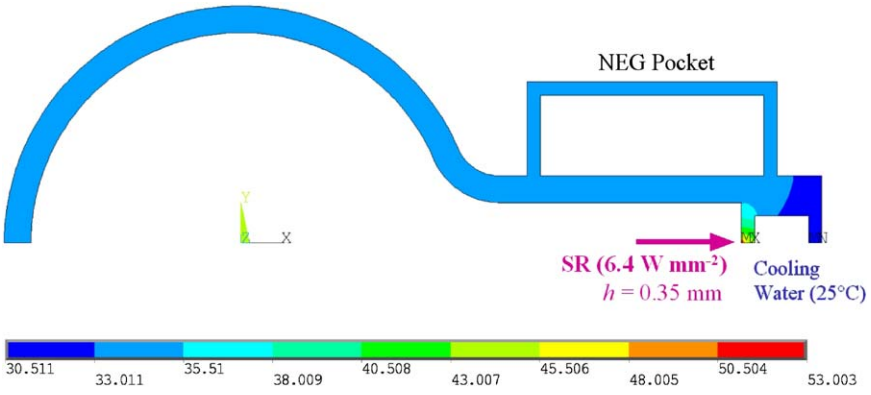

Fig. 11. Two-dimensional thermal analysis (static) of the beam duct with antechamber. The input power is 6.4 W mm^{-2} with a height (h) of 0.35 mm in the half model. The thermal conductivity of copper is 0.4 W mm^{-2} K^{-1}. The heat transfer coefficient between copper and water is 0.01 W mm^{-2} at a flow rate of about 7 l min^{-1}, and that between copper and atmosphere is about 5×10^{-6} W mm^{-1} assuming a natural air flow. The reference temperature is 25 °C.

gas desorption by the electron bombardment increased. Another possible reason is that the photoelectrons began to hit a new surface by switching off the solenoid field. The pressure decreased smoothly again after that.

One problem observed during scrubbing was pressure bursts at the test chambers. Pressure bursts on the order of 10^{-5}–10^{-6} Pa in a few seconds have been observed during beam operation. Almost all bursts occurred at a beam current larger than 1 A. The histories of the pressures for about one month (six weeks) from the beginning of the beam test (after switching the solenoid off in the case of Type-1) are shown in Figs. 13(a) and (b) for the case of Type-1 and Type-2, respectively. The plot includes pressure bursts higher than 50% of the base pressures. The bursts were prominent for Type-1 compared with Type-2. Especially, in the case of Type-1, the burst frequently accompanied a beam loss or an abort. For several hundreds of microseconds before a beam abort, the beam began to decrease, and finally aborted by the signals of the beam-loss monitors. As can be seen in the figure, the burst seemed to decrease as the vacuum scrubbing proceeded as a whole.

In the case of Type-1, several measures, such as NEG activation, the grounding of NEG strips, switching on/off of solenoid and so on, have been tried, but the effects of these have not been very positive except for the permanent magnets around the beam channel at the three joints between units. One suspicion was, therefore, that a discharge (or multipactoring) had occurred at the joints, and the discharge in the beam channel sometimes affected the beam. Actually, some traces of discharge were found near to the transverse joints, as can be seen in Fig. 14. The insufficient contact at the RF bridge might have led to discharging between the gaps or a projection of gas from gaps might have caused the glow (or arc) discharge together with a beam field. The less and small pressure burst for the case of Type-2, which has no joints between units, as in the case of Type-1, supports the explanation. All of pressure burst, of course, should not be the result of a discharge. Pressure bursts will surely be observed when the SR hits a new surface by accidental beam oscillation, for example, since the test chambers are new. Although further continued investigations are required, it can be said that the joints that are likely to make gaps transverse to the beam should be avoided as much as possible for the beam duct of high-current accelerators.

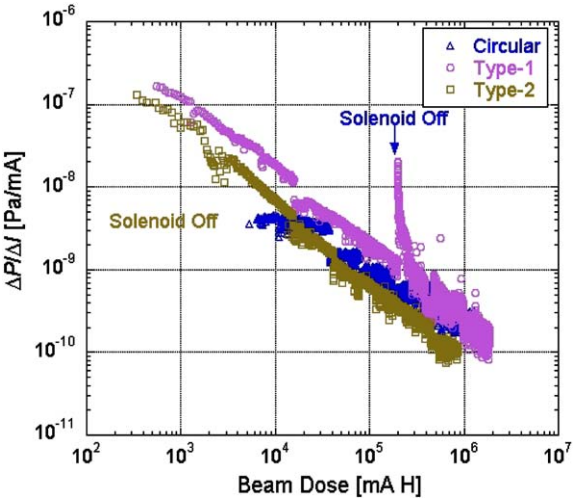

Fig. 12. Decreases of the pressure rises per unit beam current, $\Delta P/\Delta I$(Pa mA^{-1}), for both types at the test-chamber region as a function of the integrated beam current, Beam Dose [mA h].

5. Summary

Two copper test chambers with an antechamber scheme were produced with different methods, by pressing and by drawing. Each method has its merits and demerits, and further investigations are necessary concerning the manufacturing methods before mass production. The static vacuum properties of the test chambers were good. The ultimate pressure was sufficiently small, less than 3.5×10^{-9} Pa m^3 s^{-1} m^{-2} after baking. The chambers were investigated using the positron ring of the KEKB. Although the reduction of photoelectrons in the beam channel was as expected, the decrease of electrons at high currents (over 1 A) was relatively small due to the multiplication of electrons by the beam (multipactoring). Some remedy, such as a solenoid field, or any inside coating with a low secondary electron yield at the inner surface, to suppress the multiplication of

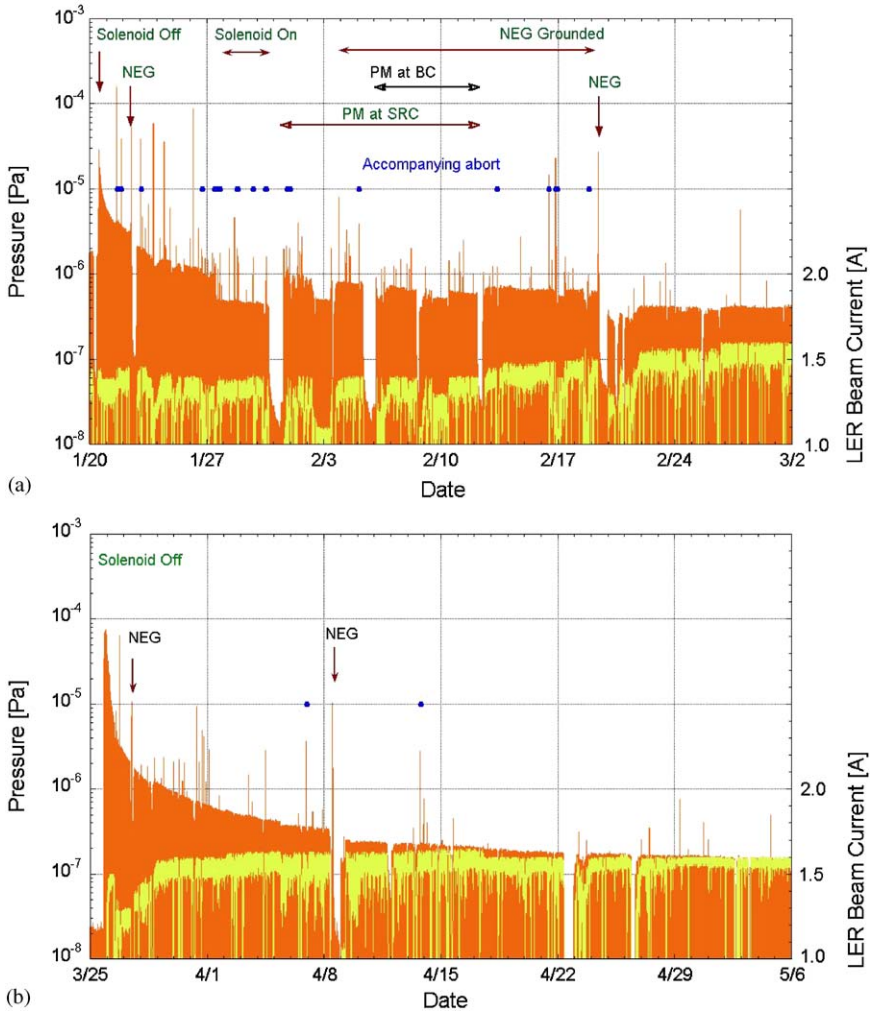

Fig. 13. History of the pressures for about one month for (a) Type-1 after switching off the solenoid field and (b) Type-2 from the beginning of beam operation, including the observed bursts larger than 50% of the base pressures at that moment. The lower line is the beam current. The dots are pressure bursts accompanying beam aborts.

electrons is indispensable for high-current operation to suppress the electron cloud effect completely. The temperature rise of the chamber is almost in agreement with the expectation, taking into account the HOM power. The vacuum scrubbing proceeded smoothly and the temperature of the chamber was reasonable. Further investigations on the pressure bursts observed during vacuum scrubbing are necessary, but it is clear that the transverse joint of the beam duct should be treated very carefully for a high-current accelerator. The next step of R&D on the beam duct will be to prepare a longer experimental region in the ring, including quadrupole and straight chambers, where the beam-position monitors and the bellows can be tested. The research of an effective coating on the inner surface of the beam channel to suppress electron multipactoring is another key issue for the future.

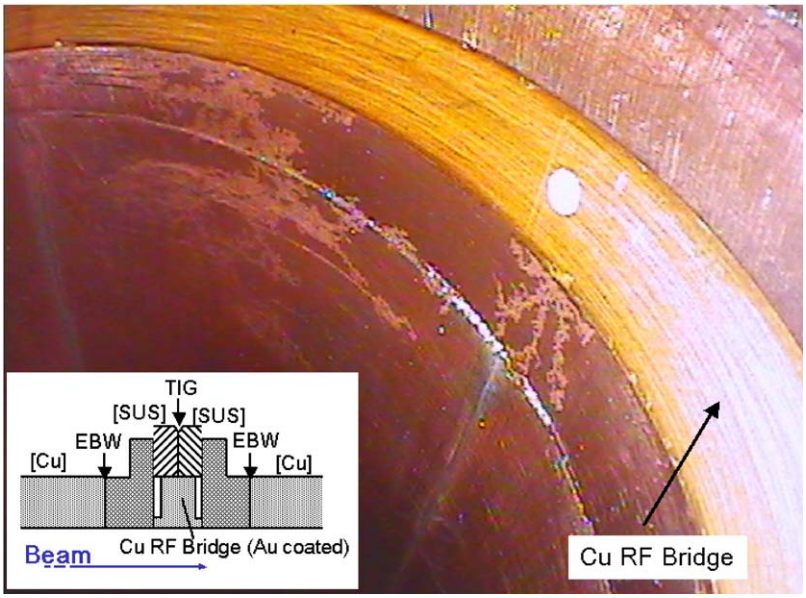

Fig. 14. Traces of discharges observed near the transverse joint part in the Type-1 test chamber after about three months of beam operation. The picture in the figure is a schematic of the structure of a joint.

Acknowledgements

The authors especially express their deep appreciation to Mr. M. Shimamoto and Mr. M. Shirai for their help during the assembling and installation of the test chambers, and to the staff members of the accelerator laboratory for their cooperation.

References

[1] Y. Onishi, KEK Proceedings 2002, 17 (2002) 1.
[2] J.T. Seemann, PAC'01, Chicago, June 18–22, 2001, p. 305.
[3] N. Toge (ed.), KEK Report 95-7, August 1995.
[4] K. Akai, et al., NIM-PR-A 499 (2003) 191.
[5] J. Seeman, et al., EPAC'02, Paris, June 3–7, 2002, p. 434.
[6] Y. Suetsugu, PAC'03, Portland (OR), May 12–16, 2003, p. 612.
[7] Y. Suetsugu, K. Shibata, K. Kanazawa, PAC'03, Portland (OR), May 12–16, 2003, p. 806.
[8] K. Kanazawa, S. Kato, Y. Suetsugu, H. Hisamatsu, M. Shimamoto, M. Shirai, NIM-PR-A 499 (2003) 66.
[9] K. Kanazawa, S. Kato, Y. Suetsugu, H. Hisamatsu, M. Shimamoto, M. Sato, M. Shirai, Appl. Surf. Sci. 169–170 (2001) 715.
[10] Y. Suetsugu, M. Tsuchiya, T. Nishidono, N. Kato, M. Satoh, S. Endo, T. Yokoyama, J. Vac. Sci. Technol. 21 (2003) 186.
[11] Y. Suetsugu, Y. Tanimoto, Y. Hori, K. Kanazawa, Y.-J. Hsu, M. Kobayashi, PAC'01, Chicago, June 18–22, 2001, p. 2177.
[12] K. Kanazawa, S. Kato, Y. Suetsugu, H. Hisamatsu, M. Shimamoto, M. Sato, M. Shirai, Appl. Surf. Sci. 169–170 (2001) 720.